

Measurement of infrared optical constants with visible photons

Anna Paterova^{1,2}, Hongzhi Yang¹, Chengwu An¹, Dmitry Kalashnikov¹, and Leonid Krivitsky^{1,*}

¹ *Data Storage Institute, Agency for Science Technology and Research (A*STAR), 138634 Singapore*

² *School of Electrical and Electronic Engineering, Nanyang Technological University, 639798*

Singapore

**email: Leonid-K@dsi.a-star.edu.sg*

Abstract

We demonstrate a new method of infrared spectroscopy with visible light sources and detectors. The technique relies on the nonlinear interference of correlated photons, produced via spontaneous parametric down conversion in a nonlinear crystal. Visible and infrared photons are split into two paths and the infrared photons interact with the sample under study. The photons are reflected back to the crystal, resembling a conventional Michelson interferometer. Interference of the visible photons is observed and it is dependent on the phases of all three interacting photons: pump, visible and infrared. The transmission coefficient and the refractive index of the sample in the infrared range can be inferred from the interference pattern of visible photons. The method does not require the use of potentially expensive and inefficient infrared detectors and sources, it can be applied to a broad variety of samples, and it does not require *a priori* knowledge of sample properties in the visible range.

Keywords

Quantum optics, Infrared spectroscopy, Parametric down conversion, Photon entanglement

Introduction

Infrared (IR) spectroscopy is a powerful tool for numerous applications including material analysis, environmental sensing, health diagnostics and others. Fourier Transform Infrared (FTIR) spectroscopy is a dominant technology in this field¹. FTIR spectrometers are available as bench top and hand held instruments, and they yield broad operation range, high spectral resolution, and fast readout. However, these instruments face challenges associated with high cost and non-ideal performance of IR-range light sources, optical components, and photon detectors.

The phenomena of nonlinear and quantum optics allow circumventing the need for IR-range components for IR spectroscopy. For the case of up-conversion spectroscopy, two visible range lasers (one with a fixed frequency, and one with a tunable frequency) are mixed in a nonlinear crystal to produce a difference frequency signal in the IR range^{2,3}. The IR signal is then used to probe the transmission of a sample and is converted back to the visible range using a frequency up-conversion crystal. One major disadvantage of this method is the requirement of sophisticated tunable lasers and multichannel detection systems.

Another approach uses the effect of nonlinear interference of photons produced via spontaneous parametric down conversion (SPDC)^{4,5,6,7,8,9,10}. In SPDC, a photon from the pump laser decays into a pair of correlated photons in a nonlinear medium. The nonlinear interferometer consists of two nonlinear crystals, arranged in such a way that down-converted photons from both crystals are superimposed. Although the photons may have different wavelengths, the interference pattern of the signal photons depends on the phase and transmissivity of the idler photons. Mandel and colleagues discovered this effect, which is now known as induced coherence^{4,5}. Recently several works have demonstrated the application of this technique for imaging^{9,10}, metrology¹¹ and spectroscopy^{6,7,12,13,14}.

In the earlier nonlinear spectroscopy schemes two nonlinear crystals were set sequentially into a common pump beam^{6,7}. A sample was placed between the crystals and all the three photons (pump, signal, and idler) traveled through it. The absorption spectrum of the sample in the IR was inferred from the interference of visible photons. The method does not require the use of IR equipment, but it has several practical limitations. For example, the sample has to be transparent to both signal and pump photons, sample's optical properties at these wavelengths have to be known in advance, and there is a risk that the pump laser damages the sample.

In this work, we introduce an alternative approach to IR spectroscopy with visible light, which is free of the limitations mentioned above. We build a setup in the form of a nonlinear Michelson interferometer, where signal (in the visible range) and idler (in the IR range) photons are split using a dichroic beam splitter and then reflected back into the crystal by two mirrors, see Figure 1. The sample under test is placed into the path of IR photons, and it modifies the interference pattern for visible photons. We infer the transmission coefficient of the sample and its refractive index in the IR-range from the modified interference pattern of visible photons. Our approach is appealing from the practical standpoint as it eliminates the limitations of the earlier methods. The work further adds to the number of optical characterization techniques, which benefit from quantum enhancement effects^{15,16,17,18,19,20}.

Materials and Methods

Theory

Let us consider the experimental scheme in Figure 1, which represents a nonlinear version of the Michelson interferometer. At the first pass through a nonlinear crystal, the pump creates a pair of correlated photons in the visible (signal) and IR (idler) range. Due to energy conservation and phase matching requirements, the frequencies ω_j and the wave vectors \vec{k}_j of the down-converted photons are given by²¹:

$$\omega_p = \omega_s + \omega_i; \vec{k}_p = \vec{k}_s + \vec{k}_i + \Delta\vec{k}, \quad (1)$$

where indices $j = i, s, p$ correspond to idler, signal and pump photons respectively, and $\Delta\vec{k}$ is a wave vector mismatch. The state vector in the first-order approximation of the perturbation theory can be written as^{22,23}:

$$|\psi\rangle_{SPDC} = |vac\rangle + \eta \sum_{k_s, k_i} F(\vec{k}_s, \vec{k}_i) a_s^+ a_i^+ |vac\rangle, \quad (2a)$$

$$F(\vec{k}_s, \vec{k}_i) = \int_{\nu} \chi(\vec{r}) E_p(\vec{r}) \exp[i\Delta k \vec{r}] d^3\vec{r}, \quad (2b)$$

where $\eta \ll 1$ is the SPDC conversion factor; a_s^+ , a_i^+ are photon creation operators for signal and idler modes respectively; $F(\vec{k}_s, \vec{k}_i)$ is the two-photon field amplitude, $E_p(\vec{r})$ is the classical pump field, which is assumed to be a monochromatic plane wave, and $\chi(\vec{r})$ is the nonlinear susceptibility of the crystal. The integral in Equation (2b) is taken over the interaction volume in the crystal ν . It can be calculated in the approximation of a uniform ($\chi(\vec{r}) = const$) and an infinite (in the transverse direction) crystal^{24, 25}:

$$F(\vec{k}_s, \vec{k}_i) \propto E_0 \int_0^L dz e^{i\Delta k_z z} \propto E_0 \text{sinc}\left(\frac{\Delta k_z L}{2}\right), \quad (3)$$

where L is the length of the crystal, E_0 is the amplitude of the pump beam, z is the axis along the pump beam, Δk_z is the projection of the wave vector mismatch onto the z axis.

For simplicity let us consider a single spatial and frequency mode of signal and idler photons. Then the state vector of a photon pair, created at the first pass of the pump beam through a nonlinear crystal, can be written as: $|\psi\rangle_0 \propto \eta_1 E_{01} |1\rangle_{s1} |1\rangle_{i1}$. Next, down-converted photons are split using a dichroic mirror and reflected back to the crystal by the mirrors. Pump and signal photons propagate together. The reflected pump beam generates SPDC photons at the second pass with the state vector given by $|\psi\rangle_2 \propto e^{i\varphi_p} \eta_2 E_{02} |1\rangle_{s2} |1\rangle_{i2}$, where φ_p is the phase acquired by the pump^{26, 27, 28}.

Let us consider the case when a medium of interest is inserted into the path of idler photons. Then the corresponding state vector $|\psi\rangle_0$ after reflection back and double pass through the medium is modified as follows^{4, 5, 9}:

$$|\psi\rangle_1 = |\tau_i|^2 e^{i(\varphi_s + \varphi_i)} \eta_1 E_{01} |1\rangle_{s1} |1\rangle_{i1} + \sqrt{1 - |\tau_i|^4} \eta_1 E_{01} |1\rangle_{s1} |1\rangle_{i_0}, \quad (4)$$

where $\varphi_{s,i}$ are the phase shifts for the signal and idler photons respectively, τ_i is an amplitude transmission coefficient of idler photons for a single pass through the medium. The parameter $\sqrt{1 - |\tau_i|^4}$ accounts for losses in the system, where idler photons are converted into all lossy modes i_0 , due to reflection, scattering or absorption.

Let us assume that photons generated at the first and the second passes of the pump are in the same mode: $|1\rangle_{s1} = |1\rangle_{s2} = |1\rangle_s$ and $|1\rangle_{i1} = |1\rangle_{i2} = |1\rangle_i$. Assuming that the interferometer arms are equal, the final state is given by the superposition:

$$|\Psi\rangle \propto \left(\eta_1 E_{01} |\tau_i|^2 e^{i(\varphi_s + \varphi_i)} + \eta_2 E_{02} e^{i\varphi_p} \right) |1\rangle_s |1\rangle_i + \eta_1 E_{01} \sqrt{1 - |\tau_i|^4} |1\rangle_{s1} |1\rangle_{i0}. \quad (5)$$

From Equation (5) the probability amplitude to detect signal photons is:

$$P_s = \langle \Psi | a_s^+ a_s | \Psi \rangle \propto |\eta_1|^2 I_{p1} + |\eta_2|^2 I_{p2} + 2|\eta_1 \eta_2| \sqrt{I_{p1} I_{p2}} |\tau_i|^2 \cos(\varphi_s + \varphi_i - \varphi_p), \quad (6)$$

where $I_{p1, p2} \equiv |E_{01, 02}|^2$ are the intensities of pump beams.

To account for the SPDC natural bandwidth, we introduce a spectral amplitude $F_\omega(\omega_s - \Omega, \omega_i + \Omega)$, which is obtained from Equation (3) by the decomposition of Δk_z ^{12,18}. Here, Ω is the detuning from the central frequencies $\omega_{s,i}$, and $2\pi \int d\Omega |F_\omega(\omega_s - \Omega, \omega_i + \Omega)|^2 = 1$. Then, the correlation function of the SPDC field $\mu(\Delta t)$ is given by^{4, 5, 29}:

$$\mu(\Delta t) = 2\pi \int_0^\infty d\Omega |F_\omega(\omega_s - \Omega, \omega_i + \Omega)|^2 e^{-i\Omega \Delta t}, \quad (7)$$

where Δt is the time delay between signal and idler photons in the interferometer.

The correlation function reaches its maximum value of unity when the optical path lengths of signal and idler photons are the same, see Figure 1:

$$n_s L + n'_s L'_s = n_i L + n'_i L'_i, \quad (8)$$

where $n_{s,i}$ are the refractive indices of the nonlinear crystal at signal and idler wavelengths, $n'_{s,i}$ are the refractive indices of the medium at signal and idler wavelengths, and $L'_{s,i}$ are the path lengths for signal and idler photons in the interferometer.

As the photon pairs are generated from the same crystal, the conversion factors can be assumed equal $\eta_1 = \eta_2 = \eta$. Taking into account the correlation function $\mu(\Delta t)$ and assuming that the transmission of the medium is constant within the SPDC linewidth, Equation (6) takes the following form:

$$P_s \propto \left(1 + \frac{2\sqrt{T_p}}{1 + T_p} |\mu(\Delta t)| |\tau_i|^2 \cos(\varphi_s + \varphi_i - \varphi_p) \right), \quad (9)$$

where $T_p = I_{p2} / I_{p1}$ is the intensity transmission coefficient of the pump. If the phases of the signal and of the pump photons are fixed, then the variation of the intensity P_s is determined by the phase

of the idler photons $\Delta\varphi_i = 2\frac{2\pi n'_i}{\lambda_i} \Delta x$, where λ_i is the idler photon wavelength, and Δx is the displacement of the IR mirror. Then the visibility of the interference fringes is given by:

$$V = \frac{P_s^{max} - P_s^{min}}{P_s^{max} + P_s^{min}} = \frac{2\sqrt{T_p}}{1 + T_p} |\mu(\Delta t)| |\tau_i|^2. \quad (10)$$

From Equation (10) it follows that the transmission coefficient of the idler (IR) photons through the medium can be inferred from the visibility of interference of signal photons detected in the visible range.

The experimental procedure for measuring the transmission spectra of the medium is as follows. First, we equalize the interferometer arms and measure the interference with the air as a reference medium $n'_{s,i} = n_{s,i}^{air} = 1$. From the measurements of the interference visibility V_{ref} we infer the total intrinsic losses of our system $|\tau_{app}|^2$, see Equation (10). Then we insert the medium of interest. We align the interferometer arms to compensate the incurred delay:

$$\Delta L' = 2(n'_i - n_i^{air})L_m, \quad (11)$$

where L_m is the thickness of the medium. Then we measure the interference visibility again and infer its relative change, see Equation (10):

$$\frac{V}{V_{ref}} = \frac{|\tau_{app}|^2 |\tau_i|^2}{|\tau_{app}|^2} = |\tau_i|^2 \equiv T_i, \quad (12)$$

We infer the refractive index and the transmission coefficient of the medium in the IR from the change of the optical path, and the visibility, respectively, see Equations (11), (12). From the obtained values, we infer the absorption α_i and reflection R_i coefficients of the medium at the corresponding wavelength:

$$V \propto |\tau_i|^2 = \left((1 - |r_i|^2) e^{-\frac{\alpha_i L_m}{2}} \right)^2 = (1 - R_i)^2 e^{-\alpha_i L_m}, \quad (13a)$$

$$|r_i|^2 \equiv R_i = \left(\frac{n'_i - n_i^{air}}{n'_i + n_i^{air}} \right)^2, \quad (13b)$$

where r_i is the amplitude reflection coefficient at normal incidence.

Experiment

Our experimental setup is shown in Figure 2. We use a continuous wave laser at 532 nm as a pump (Laser Quantum Torus, power 150 mW). The coherence length of the laser is about 100 meters. A dichroic mirror DM₁ (Semrock) reflects the pump beam to the nonlinear interferometer and transmits the signal photons in the range of 562-950 nm. The nonlinear Michelson interferometer consists of a MgO:LiNbO₃ crystal ($L=0.5$ mm; Dayoptics), a gold coated dichroic mirror DM₂ (ISP Optics), and two spherical mirrors ($f=50$ mm, Thorlabs): one is silver coated (M_s), and another one is gold coated (M_i).

The pump beam is focused into the crystal by the lens F_1 ($f=200$ mm). Signal (visible) and idler (IR) photons are generated via type-I ($e \rightarrow oo$) collinear frequency non-degenerate SPDC. The tuning of the central wavelength of the down-converted photons is performed by tilting the crystal. The idler photon wavelength is inferred from the wavelength of signal photons according to Equation (1). The dichroic mirror DM_2 reflects the idler photons and transmits the pump and signal photons.

The visibility of the interference depends on the spatial overlap of the interfering photons^{9, 30}. The intrinsic divergence of the SPDC results in different phases acquired by transverse components of wave vectors, which reveals itself in a prominent ring structure^{7, 10}. To circumvent this problem, we focus the pump beam inside the crystal, so that the divergence of down-converted photons is defined by the divergence of the pump beam. We use spherical mirrors $M_{s,i}$, positioned at a distance of their curvature radius from the crystal to form a one-to-one image of the pump waist in the crystal. Use of metallic spherical mirrors eliminates the problem of the chromatic dispersion. In this way, SPDC beams produced in two paths can be perfectly overlapped.

In the detection part, signal photons are separated from the pump by the dichroic mirror DM_1 and the notch filter NF (Semrock). The signal photons are then collimated by a lens F_2 ($f=200$ mm). The interference pattern can be detected in two ways:

1. Beams of signal photons are detected using a silicon CCD camera (Andor, iXon3 897). The CCD is located at the focal plane of the lens F_3 ($f=500$ mm), and it images the beam of signal photons. Measurements with the CCD camera facilitate alignment of the setup.
2. Signal photons emitted collinearly to the pump beam are detected by a single photon avalanche photodiode (APD, Perkin Elmer) preceded by a home-built monochromator. The monochromator allows performing wavelength selective measurements (resolution 0.25 nm) at different wavelengths of signal photons.

For the course alignment of the interferometer, the mirror M_i is translated using a motorized translation stage until a clear interference pattern is observed on the CCD. Then, signal photons are directed to the APD bypassing the monochromator. The dependence of the intensity on the optical path difference with and without the sample is measured by translating the mirror M_i . From the shift of the maxima of the interference pattern, we infer the refractive index of the sample in the IR range according to Equation (11).

Then, we perform a fine scan of the interference fringes with and without the sample. Signal photons are spectrally filtered by the monochromator and detected by the APD. We translate the mirror M_i using a piezo actuator (Thorlabs) and measure visibility of the fringes. We infer the transmission coefficient of the sample at the wavelength of idler photon according to Equation (12).

Results and discussion

We apply our technique to study four different samples: polydimethylsiloxane (PDMS), BK7 glass and pure silicon windows with and without anti-reflection (AR) coating (Edmund Optics). For proof-of-concept demonstration of our technique we chose the spectral range within 2100-2900 nm,

which corresponds to the observation of signal photons at the range of 710-655nm. The spectral range of our technique is defined by the transparency range of the LiNbO₃ crystal (0.4-5 μm).

First, we measure the interference pattern without the sample. The dependence of APD photocounts on the position of the mirror M_i is shown in Figure 3 (black squares). We fix the position at the point, where the visibility is maximized, and proceed with the fine scan using the piezo actuator. Black squares show the interference fringe detected by the APD, see inset in Figure 3. Note that the period of the fringes corresponds to the wavelength of idler photons, which agrees with the theoretical prediction, see Equation (9). Without a sample, the visibility is about 14±2%. The main factor, which limits the visibility of the interference is the imperfection of the optical elements. From our independent measurements of the DM₂, we found that for the IR light (2100-2900 nm) the reflection is 20% and for the visible light (650-750 nm) the transmission is 70%. The nonlinear crystal has the absorption of about 20%. From Equation (10) we estimate that the expected visibility is about 15%, which is in agreement with our experiment. Note that further improvements in the visibility are possible by optimization of coatings and materials of optical elements.

Next, we insert a sample (PDMS, ~140 μm thick) in the IR beam. The interference pattern shifts and its visibility is reduced, see Figure 3 (red circles). We translate the mirror M_i for approximately 120 μm to recover the interference. Then we select the wavelength by the monochromator and perform a fine scan of the interference fringes, see inset in Figure 3 (red circles). From the change of optical path length, we infer the refractive index of PDMS in the IR range, see Table 1. From the visibility of the inference fringes, we infer the transmission coefficient, see Figure 4a. In a similar way, we collect the data at different wavelengths. The tunability is achieved by rotating the crystal and selecting the signal photon wavelength by the monochromator. The data is collected with the step of 1 nm for signal photons, which corresponds to the step of 10 nm for idler photons. The obtained transmission spectrum of the PDMS sample is shown in Figure 4a. The obtained spectrum is in good agreement with the data for the same sample obtained with a commercial IR spectrophotometer (Shimadzu UV-3600 Plus). The spectral resolution of our technique in the IR is ~2.5 nm at 2200 nm, which is on par with commercially available FTIR systems. It is limited by the resolution of the monochromator for visible photons (~0.25 nm). Typical data acquisition time for each data point is about 60 seconds.

We apply the same measurement procedure for BK7 glass, and AR coated and non-coated silicon samples. The measured transmission spectra are shown in Figures 4b, 4c, 4d, respectively. Blue squares correspond to the data obtained by our method, and red lines show the data obtained using the commercial IR spectrophotometer. The two sets of data are in good agreement, which proves the validity of our technique.

Data on the refractive indices are summarized in Table 1 and they are in good agreement with the literature (<https://refractiveindex.info/>). The accuracy of the refractive index measurements is $\Delta n_i = 0.04$ and of the transmissivity is $\Delta T_i = 0.03$. Reflection and absorption coefficients are calculated by Equation (13) using the obtained refractive index and transmission coefficient data, see Table 2. According to Equation (13), the accuracy of the reflection coefficient is $\Delta R_i = 0.01$ and the accuracy of the absorption coefficient is $\Delta \alpha_i = 0.06 \text{ cm}^{-1}$.

Conclusions

In conclusion, we have developed the method for measuring optical constants in the mid-IR range through measurements of the interference of visible photons. The method allows the calculation of refractive index, transmission, reflection and absorption of samples in a broad spectral range with good accuracy and spectral resolution. The method is based on the nonlinear interference of correlated photons produced via SPDC. The main feature of this technique is that idler and signal photons are separated in the interferometer, which allows measuring properties of the medium at the IR range without prior information about its properties at the visible range. The method is demonstrated with several samples, including samples which are opaque in the visible range. Results are in good agreement with data obtained using conventional IR spectroscopy technique and literature data. This work paves the way for further practical adoption of the method in the field of IR optical characterization, without resorting to IR grade detectors and sources.

Acknowledgements

The work is supported by DSI core funding. The authors thank D. H. Zhang, G. Vienne, R. Bakker and S. Kulik for stimulating discussions. A.P. would like to acknowledge the support of the SINGA PhD fellowship.

References

1. Smith BC. Fundamentals of Fourier Transform Infrared Spectroscopy. *CRC Press*, 2011.
2. Heilweil EJ. Ultrashort-pulse multichannel infrared spectroscopy using broadband frequency conversion in LiIO_3 . *Optics Letters* 1989; **14**: 551-553.
3. Dougherty TP, Heilweil EJ. Dual-beam subpicosecond broadband infrared spectrometer. *Optics Letters* 1994; **19**: 129-131.
4. Zou XY, Wang IJ, Mandel L. Induced coherence and indistinguishability in optical interference. *Phys Rev Lett* 1991; **67**: 318-321.
5. Wang IJ, Zou XY, Mandel L. Induced coherence without induced emission. *Phys Rev A* 1991; **44**: 4614-4622.
6. Kalashnikov DA, Paterova AV, Kulik SP, Krivitsky LA. Infrared spectroscopy with visible light. *Nature Photonics* 2016; **10**: 98-101.
7. Paterova AV, Lung S, Kalashnikov DA, Krivitsky LA. Nonlinear infrared spectroscopy free from spectral selection. *Scientific Reports* 2017; **7**: 42608.
8. Chekhova MV, Ou ZY. Nonlinear interferometers in quantum optics. *Adv in Opt & Pht* 2016; **8**: 104-155.
9. Lemos GB, Borish V, Cole GD, Ramelow S, Lapkiewicz R *et al.* Quantum imaging with undetected photons. *Nature* 2014; **512**: 409-412.
10. Hochrainer A, Lahiri M, Lapkiewicz R, Lemos GB, Zeilinger A. Interference Fringes Controlled by Non-Interfering Photons. *Optica* 2017; **4**: 341-344.
11. Hudelist F, Kong J, Liu C, Jing J, Ou ZY *et al.* Quantum metrology with parametric amplifier-based photon correlation interferometers. *Nat Comm* 2014; **5**: 3049.
12. Burlakov AV, Chekhova MV, Klyshko DN, Kulik SP, Penin AN *et al.* Interference effects in spontaneous two-photon parametric scattering from two macroscopic regions. *Phys Rev A* 1997; **56**: 3214-3225.

13. Burlakov AV, Kulik SP, Penin AN, Chekhova MV. Three-photon interference: Spectroscopy of linear and nonlinear media. *J Exp Theor Phys* 1998; **86**: 1090-1097.
14. Kulik SP, Maslennikov GA, Merkulova SP, Penin AN, Radchenko LK *et al.* Two-photon interference in the presence of absorption. *J Exp Theor Phys* 2004; **98**: 31-38.
15. Kalashnikov DA, Pan Z, Kuznetsov AI, Krivitsky LA. Quantum Spectroscopy of Plasmonic Nanostructures. *Phys Rev X* 2014; **4**: 011049.
16. Dorfman KE, Schlawin F, Mukamel S. Nonlinear optical signals and spectroscopy with quantum light. *Rev Mod Phys* 2016; **88**: 045008.
17. Ono T, Okamoto R, Takeuchi S. An entanglement-enhanced microscope. *Nat Comm* 2013; **4**: 2426.
18. Nasr MB, Saleh BEA, Sergienko AV, Teich MC. Demonstration of Dispersion-Canceled Quantum-Optical Coherence Tomography. *Phys Rev Lett* 2003; **91**: 083601.
19. Teich MC, Saleh BEA, Wong FNC, Shapiro JH. Variations on the Theme of Quantum Optical Coherence Tomography: A Review. *Quant Inf Process* 2012; **11**: 903-923.
20. Samantaray N, Ruo-Berchera I, Meda A, Genovese M. Realization of the first sub-shot-noise wide field microscope. *Light: Science & Applications* 2017; **6**: e17005.
21. Klyshko DN. Photon and Nonlinear Optics. *Gordon & Breach Science Pub*, 1988.
22. Belinsky AV, Klyshko DN. Two-Photon Wave Packets. *Laser Physics* 1994; **4**: 663-689.
23. Mikhailova YM, Volkov PA, Fedorov MV. Biphoton wave packets in parametric down-conversion: Spectral and temporal structure and degree of entanglement. *Phys Rev A* 2008; **78**: 062327.
24. Monken CH, Souto Ribeiro PH, Pádua S. Transfer of angular spectrum and image formation in spontaneous parametric down-conversion. *Phys Rev A* 1998; **57**: 3123-3126.
25. Walborn SP, de Oliveira AN, Pádua S, Monken CH. Multimode Hong-Ou-Mandel Interference. *Phys Rev Lett* 2003; **90**: 143601.
26. Klyshko DN. Ramsey interference in two-photon parametric scattering. *J Exp Theor Phys* 1993; **104**: 2676-2684.
27. Korystov DY, Kulik SP, Penin AN. Rozhdestvenski hooks in two-photon parametric light scattering. *Jetp Lett* 2001; **73**: 214-218.
28. Heuer A, Raabe S, Menzel R. Phase memory across two single-photon interferometers including wavelength conversion. *Phys Rev A* 2014; **90**: 045803.
29. Baek S-Y, Kim Y-H. Spectral properties of entangled photons generated via type-I frequency-nondegenerate spontaneous parametric down-conversion. *Phys Rev A* 2009; **80**: 033814.
30. Grayson TP, Barbosa GA. Spatial properties of spontaneous parametric down-conversion and their effect on induced coherence without induced emission. *Phys Rev A* 1994; **49**: 2948-2961.

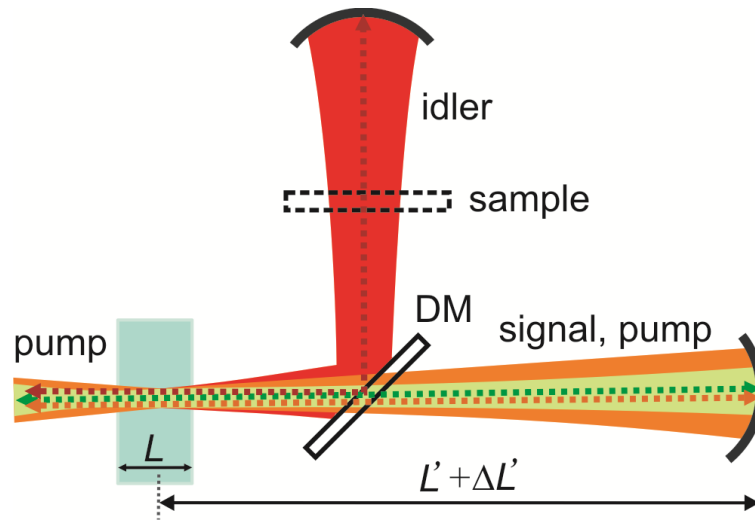


Figure 1 A nonlinear version of a Michelson interferometer. Signal and idler photons are generated via SPDC in a nonlinear crystal. The idler photon (IR) is separated from the signal and pump photons (visible) by a dichroic mirror (DM). Spherical mirrors are positioned at a distance of $L' = 2F'$ from the crystal, where F' is the focal lengths of the mirrors. The sample is inserted in the path of the idler photon. $\Delta L'$ is the optical path lengths difference between the arms. The interference pattern of signal photons is detected at the output of the interferometer.

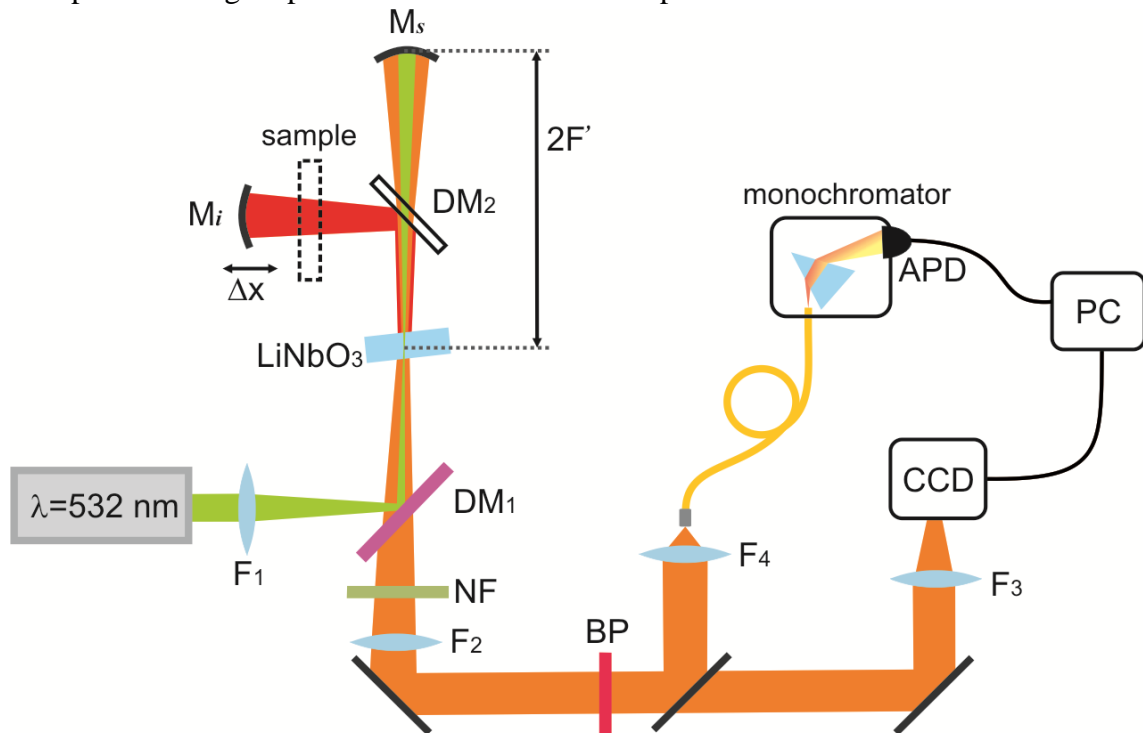


Figure 2 The experimental setup. A CW-laser at 532 nm is used as a pump for a LiNbO₃ crystal, where SPDC photons are generated. Idler photons are reflected by the dichroic mirror DM₂, while signal and pump photons pass through the mirror. Spherical mirrors M_s and M_i with focal distance F' reflect the photons back into the crystal. A sample is placed in the IR arm of the interferometer between DM₂ and M_i. The interference pattern is captured either by a CCD camera or by a single photon detector (APD) preceded by a monochromator. NF is a notch filter; BP is a band pass filter.

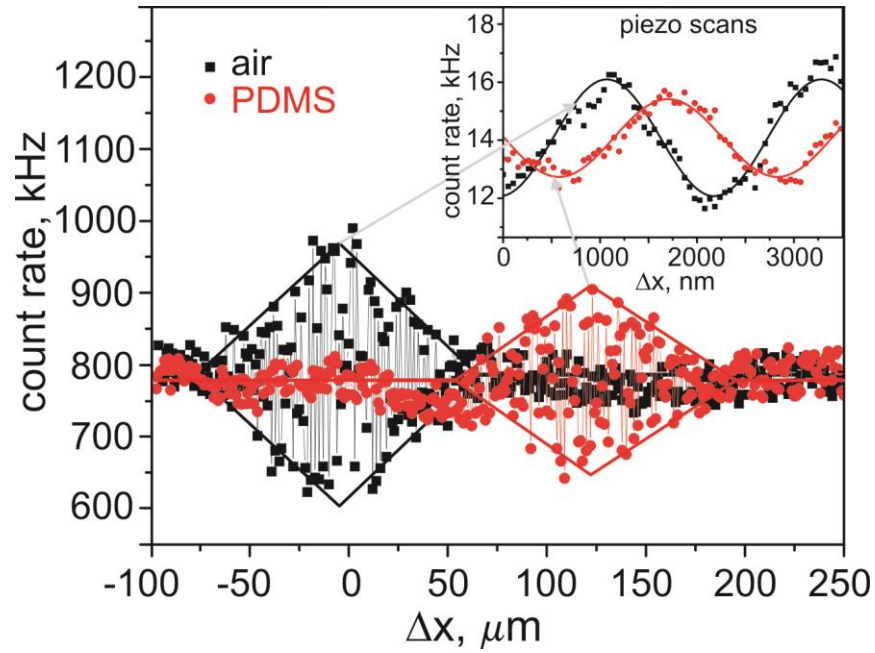


Figure 3 Dependence of the photocount rate of the APD on the position of the mirror M_i . Black squares show the data with the air, and red circles show the data obtained with a 143 μm thick PDMS sample. The inset shows the interference fringes observed by fine translation of the mirror M_i using a piezo actuator. Solid lines show data fitted by Equation (7); for the inset the fitting function is the cosine-function according to Equation (9).

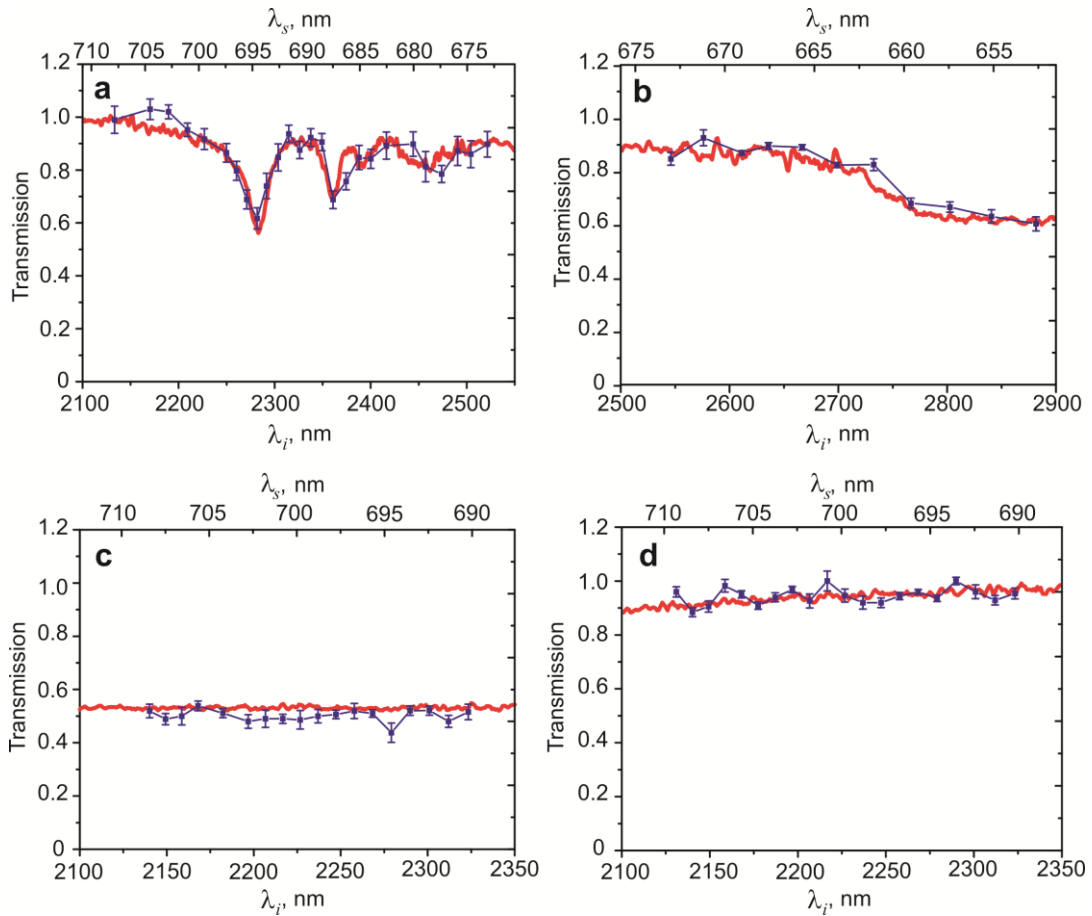


Figure 4 Transmission spectra of a 143 μm thick PDMS sample (a), a 1 mm thick BK7 sample (b), a 1 mm thick silicon sample without AR coating (c), and a 1 mm thick silicon sample with AR-

coating (d). The blue squares show the experimental results obtained by our method, the red curves show the data obtained with a commercial IR spectrophotometer. The top axis indicates the actual measurement wavelength of signal photons and the bottom axis indicates wavelength of idler photons calculated using Equation (1). Error bars in (a)–(d) show \pm s.d.

Table 1 Values of the refractive index and transmittance (mean \pm s.d.) of the samples calculated from the measurements shown in Figures 3, 4 and using Equations (11), (12)

Sample (thickness, μm)	wavelength, nm	Refractive index, n_i'		Transmittance, T_i	
		our method	database	our method	conventional method
PDMS (143)	2200	1.41 \pm 0.02	1.39	0.94 \pm 0.02	0.94
BK7 (980)	2600	1.51 \pm 0.03	1.49	0.87 \pm 0.02	0.88
Si / w/o AR (1030)	2200	3.50 \pm 0.07	3.45	0.49 \pm 0.04	0.52
Si/ w AR (1050)				0.95	0.94

Table 2 Calculated reflectance and absorption coefficients (mean \pm s.d.) of the samples using Equation (13)

Sample	wavelength, nm	Reflectance, R_i		Absorption, α_i cm $^{-1}$	
		our method	database	our method	conventional method
PDMS	2200	0.030 \pm 0.003	0.027	0.67 \pm 0.06	0.69
BK7	2600	0.041 \pm 0.004	0.038	0.57 \pm 0.06	0.51
Si /w/o AR	2200	0.31 \pm 0.01	0.30	0.00 \pm 0.05	0.00
Si/ w AR		0.025 \pm 0.005	0.030	0.00 \pm 0.01	0.00